Lithium Dynamics in $LiMn_2O_4$ Probed Directly by Two-Dimensional ^7Li NMR

V. W. J. Verhoeven,[1] I. M. de Schepper,[1] G. Nachtegaal,[2] A. P. M. Kentgens,[2]
E. M. Kelder,[3] J. Schoonman,[3] and F. M. Mulder[1]

[1]*Interfaculty Reactor Institute, Delft University of Technology, Mekelweg 15, 2629 JB Delft, The Netherlands*
[2]*Department of Physical Chemistry/Solid-State NMR, NSR Center, University of Nijmegen, Toernooiveld 1, 6525 ED Nijmegen, The Netherlands*
[3]*Laboratory for Inorganic Chemistry, Delft University of Technology, Julianalaan 136, 2628 BL Delft, The Netherlands*

(Received 25 October 2000)

$LiMn_2O_4$ has been studied using magic-angle-spinning nuclear magnetic resonance (MAS NMR). 1D MAS NMR shows three Li resonances assigned to different crystallographic sites. At low temperatures an extra peak appears, indicating charge ordering of Mn^{3+} and Mn^{4+}. Direct observation of the lithium dynamics was possible using rotor-synchronized 2D exchange NMR. A millisecond time scale exchange of lithium starts around 285 K between the 8*a* and the 16*c* site. At 380 K lithium even starts to hop between more than two sites. The activation energies and Li jump rates are derived and are in agreement with those determined macroscopically.

DOI: 10.1103/PhysRevLett.86.4314 PACS numbers: 66.30.Hs, 61.18.Fs, 81.05.Je, 82.56.Fk

$LiMn_2O_4$ has attracted substantial interest in the past few years, as it is a very promising cathode material for advanced Li-ion batteries. The material has a high energy capacity per unit weight, is cheap, and contains no heavy or poisonous metals, hence it is environmentally friendly compared to materials used in today's Ni-Cd and lead-acid batteries. The first pilot battery production lines are in operation.

Rodríguez-Carvajal *et al.* [1] have shown that a Mn^{3+}, Mn^{4+} charge ordering takes place below RT. Fong *et al.* [2] described the crystal structure of $LiMn_2O_4$ for $x = 1$ and $x = 0.2$. Wills *et al.* [3] reported the crystal structure of $LiMn_2O_4$ at low temperatures and on the magnetic properties of the material. Berg *et al.* [4] noted that some of the Li is located on interstitial 16*c* sites. Thackeray *et al.* [5] and Mishra *et al.* [6] reported the structural stability of $LiMn_2O_4$. Xia *et al.* [7] studied the capacity fading of a battery using $LiMn_2O_4$ as a cathode. A fundamental and crucial property of the material is its ability to conduct Li ions through the crystal. To the best of our knowledge no microscopic techniques have been able to observe this Li mobility directly. Here, we present measurements of the lithium mobility, diffusion pathway, and atomic site occupancies observed in $Li[Mn_{1.96}Li_{0.04}]O_4$ as a function of temperature by using solid state nuclear magnetic resonance (NMR) techniques.

To study the dynamics of lithium in $LiMn_2O_4$ on a ms time scale, two-dimensional rotor-synchronized exchange NMR has been used [8–10]. The technique gives an unambiguous and direct answer to the question of whether lithium is hopping between two different sites or not and on which time scale. This study is of a similar nature as that of Xu *et al.* [11] on Li transport in Li_4SiO_4. Several NMR studies on chemical properties of $LiMn_2O_4$ have been reported using one-dimensional NMR. Gee *et al.* [12] studied the influence of substituting a small percentage of Mn by Li, Co, or Ni. Lee *et al.* [13] used NMR to characterize sample preparation procedures. Koiwai *et al.* [14] reported the magnetic properties of $LiMn_2O_4$ using ^{7}Li-NMR. Mustarelli *et al.* [15] used NMR and XRD to study the structure of $LiMn_2O_4$.

In the study presented here, ^{7}Li MAS NMR spectra were recorded using a Bruker DMX-300 spectrometer operated at a frequency of 116 MHz. A 2.5 mm MAS probe spinning at 28 kHz was employed. The temperature was stabilized within 0.5 K using a nitrogen gas flow. Temperature calibration was performed using the ^{207}Pb resonance of $Pb(NO_3)_2$ [16]. Two-dimensional exchange NMR spectra were recorded using a hardware rotor synchronization of the exchange time (also called mixing time) and by employing the whole-echo acquisition technique described in [17]. The exchange of Li between sites with different chemical shifts, i.e., crystallographically different sites, can be observed directly as cross peaks in these spectra. The evolution of the cross peak intensity as a function of time provides direct information on the rate of the exchange process. Furthermore, the temperature dependence has been analyzed using an Arrhenius plot for the jump rate versus $\frac{1}{T}$.

The materials, obtained from the company SEDEMA (Tertre, Belgium), were characterized by x-ray and neutron diffraction and were of single phase having the spinel structure (space group Fd3m) with $a = 8.24$ Å. It is well known that the $LiMn_2O_4$ compound shows a Jahn-Teller distortion and a charge ordering at $T = 280$ K [1]. In the investigated compound $Li[Mn_{1.96}Li_{0.04}]O_4$, where the atoms in front of, between, and after the brackets are on, respectively, $8a/16c$, $16d$, and $32e$ sites, no Jahn-Teller distortion was found with temperature dependent neutron powder diffraction experiments [18]. This could be expected since the random distribution of Li over the 16*d* positions prevents such a transition to an ordered state.

In Fig. 1 the ^{7}Li MAS NMR spectra of $Li[Mn_{1.96}Li_{0.04}]O_4$ are shown as a function of temperature. The

 0031-9007/01/86(19)/4314(4)$15.00

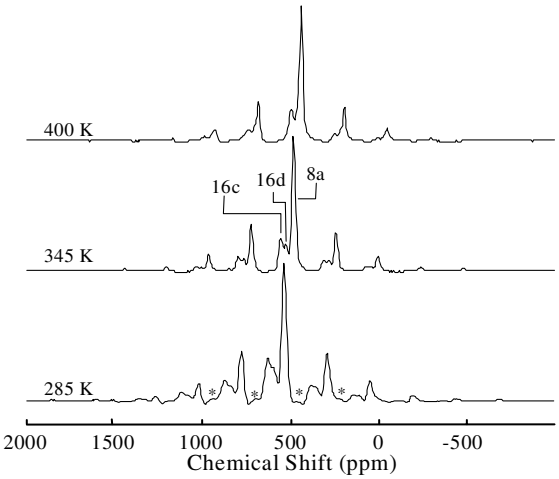

FIG. 1. ^{7}Li-MAS-NMR spectra of $Li[Mn_{1.96}Li_{0.04}]O_4$ as a function of temperature (K). The spinning speed was 28 000 ± 3 Hz (241 ppm) and a 90° pulse length of 1.7 μs was used. New peaks at 285 K are denoted by an asterisk.

strongest MAS NMR spinning sideband manifold in the spectrum is assigned to lithium on 8*a* sites, which is the lithium site with the highest occupancy as was observed in neutron diffraction [4]. The two smaller peaks belong to lithium located at the 16*d* sites and the interstitial 16*c* sites [4]. All subspectra shift to smaller ppm values, i.e., smaller hyperfine fields as the temperature increases. This was analyzed in Refs. [12] and [13] as the effect of the paramagnetic susceptibility changing proportional to $\frac{1}{T}$. The large width of the spectrum is caused by the anisotropic polarization of the paramagnetic manganese magnetic moments [15]. The width expressed in ppm was checked to be field independent, which indicates negligible quadrupole interaction. Therefore the spectrum has the shape of a central transition.

At high temperatures, i.e., 475 K, the lines start to coalesce due to motional averaging, indicating the onset of Li exchange between the different sites at a rate comparable to the distance in Hz between the different resonances. This is in agreement with the result reported by Lee *et al.* [13] indicating the same rapid exchange effect. At low temperatures, i.e., 285 K, a fourth peak appears, and additionally line broadening (+35%) of all resonances becomes clearly visible in the 1D spectrum (Fig. 1). This peak may be caused by charge ordering of Mn^{3+} and Mn^{4+} as has been reported by Rodríguez-Carvajal [1]. Such a charge ordering leads to Li surroundings with different Mn^{3+} and Mn^{4+} coordinations instead of Mn ions with all the same time-averaged +3.55 valence.

Figure 2a, in which the 2D spectrum of $Li[Mn_{1.96}Li_{0.04}]O_4$ at a temperature of 285 K is plotted, shows the absence of exchange between different sites for a mixing time of $t_{mix} = 5$ ms. It also demonstrates the good performance of the rotor-synchronized-pulse sequence which causes strong signals to be found on the diagonal and cross peaks between side bands of the same site to be

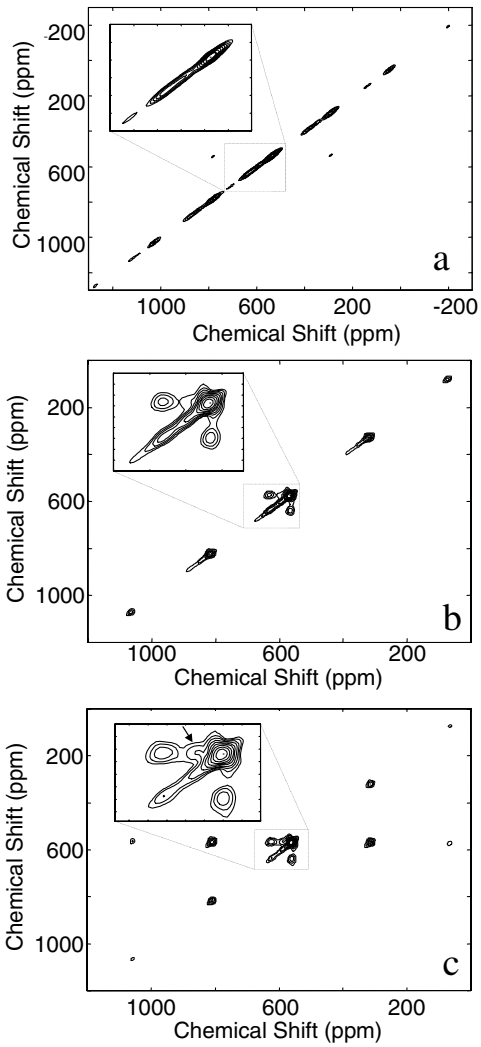

FIG. 2. 2D MAS NMR spectra of $Li[Mn_{1.96}Li_{0.04}]O_4$ (a) at 285 K with $t_{mix} = 5$ ms, (b) at 380 K with $t_{mix} = 5$ ms, and (c) $t_{mix} = 10$ ms. The spinning speed equals 28 kHz (241 ppm). The arrow marks the 8*a*-16*d* cross peak.

suppressed. Furthermore, it indicates that spin diffusion is completely absent due to the fast MAS used in these experiments. As the temperature is increased, the 2D plot (Fig. 2b) shows the onset of cross peaks for the same t_m. A gradual conversion of the diagonal peaks towards a more circular shape corresponds to Li atoms remaining at the same site, but experiencing a slight change in the environment, which is caused by other nearby Li atoms changing position. Note that intense cross peaks are observed between Li signals from Li on the 8*a* and 16*c* sites. This means that large fractions of the Li hop from highly occupied 8*a* sites to the lower occupied interstitial 16*c* sites. The signal is assigned to the 16*c* site rather than to the 16d site, since the shortest diffusion path from 8*a* to 8*a* sites leads from 8*a* to 16*c* to 8*a* in an almost straight line. The result directly indicates that Li occupies the interstitial 16*c* site for a finite amount of time. Increasing the mixing time results in increased cross peaks intensity

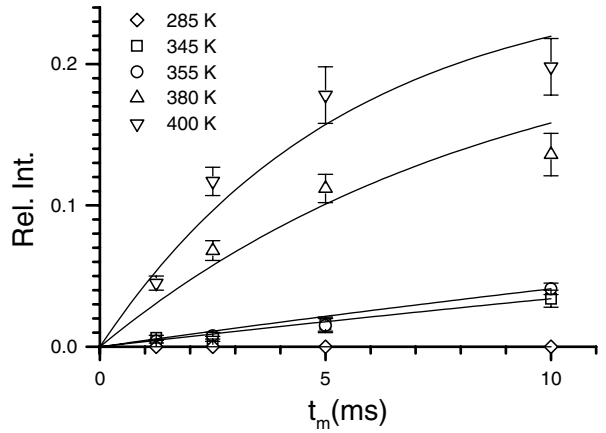

FIG. 3. The intensity of 8*a*-16*c* cross peaks as a function of mixing time (t_m) for the temperatures (K) indicated in the figure.

as can be seen in Fig. 3 where the cross peak intensity relative to the intensity of the largest peak as a function of the mixing time has been plotted. Full saturation of the cross peaks has not been achieved at this temperature as this would require a mixing time which is longer than the T_1 relaxation time ($T_1 = 10$ ms).

The data allow the extraction of two types of information. First is the direct determination of a time scale on which the Li hops from one site to another, and second is the temperature dependence of the exchange which yields in an Arrhenius analysis the activation energy of the hopping process.

Since there is mainly hopping between two sites at the time scale probed by the experiment a two-site Markov hopping process can be used to describe the data. The curves of Fig. 3 have been fitted with the function $I(t_m) = \frac{\tau_2}{\tau_1+\tau_2}[1 - e^{-(\tau_1+\tau_2/\tau_1\tau_2)t_m}]$, where $\frac{1}{\tau_1}$ and $\frac{1}{\tau_2}$ are the jump rates for Li ions hopping from 8*a* to 16*c* sites and from 16*c* to 8*a* sites, respectively. Within the model the temperature dependent ratio between τ_1 and τ_2 can be derived from the ratio of the integrated peak intensities in the 1D NMR spectra: $\frac{\tau_1}{\tau_2} = \frac{\text{intensity } 8a}{\text{intensity } 16c}$. The results of the fits are presented in Table I. From the jump rate a self-diffusion coefficient can be calculated using the formula $D = \frac{1}{4}\frac{l^2}{\tau}$ where l is the distance over which the Li-ions jump and $\frac{1}{\tau} = \frac{\tau_1+\tau_2}{\tau_1\tau_2}$ is the average jump rate. In this case $l = 1.78$ Å which leads to self-diffusion coefficients given in Table I. Note that these self-diffusion coefficients are derived by studying the movement of a single atom in an equilibrium distribution of Li in the crystals. As is explained by, e.g., Crank [19], differences between self-diffusion coefficients and chemical diffusion coefficients can be very large because the applied electric field, used to measure the chemical diffusion coefficients, can create large (local) gradients in the Li concentration, which are not present when measuring self-diffusion coefficients.

There must be a difference between the activation energies for jumping from 8*a* to 16*c* and vice versa since

TABLE I. The ratio $\frac{\tau_1}{\tau_2}$, determined using the 1D NMR spectral intensities, jump rates, and self-diffusion coefficients derived by fitting curves of Fig. 3.

T (K)	$\frac{\tau_1}{\tau_2}$	$\frac{1}{\tau_1}$ (s^{-1})	$\frac{1}{\tau_2}$ (s^{-1})	D (10^{-16} cm^2 s^{-1})
285	...	...	...	...
345	3.7 ± 0.1	1.9 ± 0.4	6.8 ± 1.3	3.4 ± 0.7
355	3.5 ± 0.1	2.3 ± 0.4	7.9 ± 1.6	4.0 ± 0.8
380	3.3 ± 0.1	13 ± 1	43 ± 4	22 ± 2
400	2.8 ± 0.1	24 ± 2	68 ± 6	36 ± 4

the sites are not equally occupied. This difference has been calculated using the temperature dependent ratio of Li-ions on 8*a* and 16*c* sites (Table I) and the Boltzmann equation, yielding a value of 700 ± 70 K. In Fig. 4 the derived jump rates $\frac{1}{\tau_i}$ have been plotted versus $\frac{1}{T}$ on a semilog scale. The activation energies for jumping from a 8*a* to a 16*c* site and vice versa are obtained from the exponents of exponential fits of the curves, and the difference of 700 K between them. The exponents of the fit are 6800 and 6100 K which corresponds in both cases, within the error bars, to an activation energy of 0.5 ± 0.1 eV. In Fig. 5 the activation energy and energy difference between the 8*a* and 16*c* sites are illustrated. Using conductivity measurements Massarotti *et al.* [20] found a value 0.4 eV for the activation energy of the Li-ion conduction process, which is in good agreement with the value found in this study using a microscopic method. We can, therefore, conclude that this microscopically determined activation energy is the main barrier for the macroscopic Li-ion transport, i.e., that the hopping on the 8*a* ⇒ 16*c* diffusion path observed in the microscopic NMR measurements corresponds to the main lithium conduction process.

As can be seen in Fig. 2c new cross peaks appear in the spectra at 380 K for a mixing time of $t_{\text{mix}} = 10$ ms. The occurrence of these new peaks indicates that secondary hopping processes are becoming prominent, i.e., there is

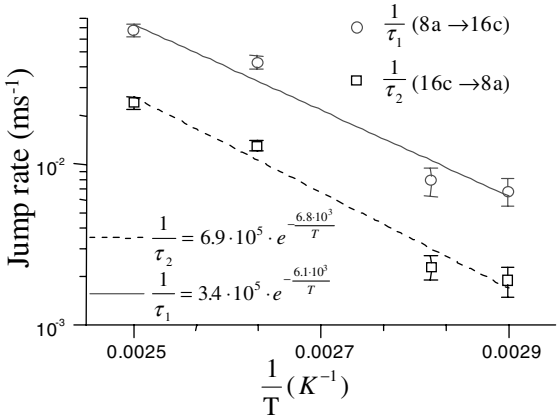

FIG. 4. Semilog plot of the derived jump rates versus $\frac{1}{T}$. Using $\frac{1}{\tau}(T) = \frac{1}{\tau}(\infty)\exp(-\frac{E}{T})$ the activation energies E are calculated to be $E = 0.5 \pm 0.1$ eV.

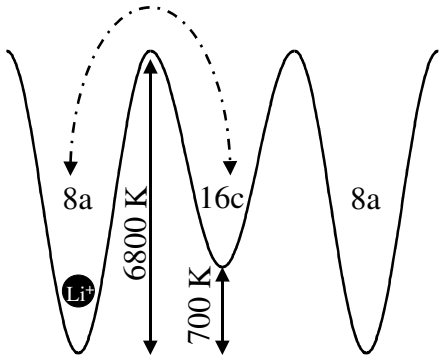

FIG. 5. Schematical plot of the activation energy and energy difference between the 8*a* and 16*c* site.

sufficient mobility to make more than one jump during t_m. This directly results in cross peaks between 8*a* spinning side bands following $8a \Rightarrow 16c \Rightarrow 8a$ hopping, since different 8*a* sites have a different orientation of the anisotropy tensor with respect to the applied field. The cross peak indicated by an arrow in Fig. 2c shows that hopping between the 8*a* and the 16*d* site also becomes an important process. The two-site model then has to be replaced by a three-site model. However, since our t_m could not be extended to sufficiently long times, it was not possible to accurately determine the three-site model parameters.

To our knowledge, this is the first time that the microscopic mobility of Li ions has been observed directly in $Li[Mn_{1.96}Li_{0.04}]O_4$ using a powerful 2D NMR technique. Temperature dependent experiments indicate an onset of lithium exchange on a ms time scale between two sites at 285 K and between more than two sites at 380 K. Line broadening and a fourth spinning-side-band manifold, which are probably caused by charge ordering of Mn^{3+} and Mn^{4+}, disappears at the same temperature as the lithium exchange starts, indicating that the charge ordering and lithium-ion dynamics are correlated. Enhanced screening of the ions in the crystal may lower the barriers for Li mobility, which is the subject of further research. The equilibrium occupation of the 8*a* and 16*c* sites and the exponential time dependence of the cross peaks yields the $8a \Rightarrow 16c$ and $16c \Rightarrow 8a$ activation energies. These activation energies of 0.5 ± 0.1 eV are in good agreement with values found in literature [20] from macroscopic methods. This indicates that the diffusion path found here is the primary Li conduction process.

This work is part of the Delft Interfaculty Research Center program "Decentralized Production and Storage of Electricity for Large-Scale Application of Renewable Energy." Financial support from the "Stichting Fundamenteel Onderzoek der Materie" is gratefully acknowledged. The "Stichting Chemische Wetenschappen" is acknowledged for their support of the NMR facilities in Nijmegen.

[1] J. Rodríguez-Carvajal, G. Rousse, C. Masquelier, and M. Hervieu, Phys. Rev. Lett. **8**, 46601 (1998).
[2] C. Fong, B. J. Kennedy, and M. M. Elcombe, Z. Kristallogr. **209**, 941 (1994).
[3] A. S. Wills, N. P. Raju, and J. E. Greedan, Chem. Mater. **11**, 1510 (1999).
[4] H. Berg, E. M. Kelder, and J. O. Thomas, J. Mater. Chem. **9**, 427 (1999).
[5] M. M. Thackeray, M. F. Mansuetto, and J. B. Bates, J. Power Sources **68**, 153 (1997).
[6] S. K. Mishra and G. Ceder, Phys. Rev. B **59**, 6120 (1999).
[7] Y. Xia, Y. Zhou, and M. Yoshio, J. Electrochem. Soc. **144**, 2593 (1997).
[8] A. F. de Jong, A. P. M. Kentgens, and W. S. Veeman, Chem. Phys. Lett. **109**, 337 (1984).
[9] A. P. M. Kentgens, E. de Boer, and W. S. Veeman, J. Chem. Phys. **87**, 6859 (1987).
[10] K. Schmidt-Rohr and H. W. Spiess, *Multidimensional Solid-State NMR and Polymers* (Acadamic Press, London, 1994).
[11] Z. Xu and J. F. Stebbins, Science **270**, 1332 (1995).
[12] B. Gee, C. R. Horne, E. J. Cairns, and J. A. Reimer, J. Phys. Chem. B **102**, 10 142 (1998).
[13] Y. J. Lee, F. Wang, and C. P. Grey, J. Am. Chem. Soc. **120**, 12 601 (1998).
[14] A. Koiwai, J. Sugiyama, T. Hioki, and S. Noda, J. Power Sources **68**, 637 (1997).
[15] P. Mustarelli, V. Massarotti, M. Bini, and D. Capsoni, Phys. Rev. B **55**, 12 018 (1997).
[16] A. Bielecki, J. Magn. Reson. **116**, 215 (1995).
[17] M. Ernst, A. P. M. Kentgens, and B. H. Meier, J. Magn. Reson. **138**, 66 (1999).
[18] V. W. J. Verhoeven, F. M. Mulder, and I. M. de Schepper, Physica (Amsterdam) **276B–278B**, 950 (2000).
[19] J. Crank, *The Mathematics of Diffusion* (Oxford Science Publications, Oxford, 1975), 2nd ed.
[20] V. Massarotti, D. Capsoni, M. Bini, G. Chiodelli, C. B. Azzoni, M. C. Mozzati, and A. Paleari, J. Solid State Chem. **13**, 941 (1997).